Article

The Golden Ratio in Nature: A Tour Across Length Scales

Callum R. Marples [1] and Philip M. Williams [2]*

[1] cmarples@hotmail.co.uk
[2] Molecular Therapeutics and Formulation, School of Pharmacy, University of Nottingham, Nottingham NG7 2RD, U.K.
* Correspondence: phil.williams@nottingham.ac.uk

Abstract: The Golden ratio is an irrational number that has a tendency to appear in many different scientific and artistic fields. It may be found in natural phenomena across a vast range of length scales; from galactic to atomic. In this review, the mathematical properties of the Golden ratio are discussed before exploring where in nature it has been found; beginning at astronomical scales and progressing to smaller lengths, until reaching those of atomic and quantum physics. In making such a tour across length scales, it is illustrated just how prevalent this single number is within the natural universe.

Keywords: Golden ratio; Irrational numbers; Fibonacci sequence; Spiral galaxy; Planetary orbits; KAM Theorem; Ultimatum game; Proteins; Penrose tiling; Quasicrystals.

1. Introduction

The *Golden ratio*, $\phi = 1.61803...$ has fascinated people of multiple disciplines, sciences and arts alike, for centuries [1–8]. The earliest known definition for ϕ appeared in Euclid's *Elements* in approximately 300 BC. The definition involves dividing a line segment into two parts, of lengths A and B as shown in Figure 1, such that the ratio of the larger part, A, to the smaller part, B, equals the ratio of the whole segment to the larger part,

$$\frac{A}{B} = \frac{A+B}{A} \tag{1}$$

This definition is an example of *self-similarity*. This means that the line segment is similar to parts of itself, with A being to $A+B$ what B is to A. If a similar division was to be made to length A, then the larger part of that cut would have length B. The common ratio is the Golden ratio, the exact value of which can be found by setting A/B equal to ϕ in Equation 1 to give a quadratic equation,

$$\phi^2 - \phi - 1 = 0 \tag{2}$$

The positive solution of this quadratic is the Golden ratio,

$$\phi = \frac{1+\sqrt{5}}{2} = 1.618\,033\,988\,749\,894\,9... \tag{3}$$

The other solution gives,

$$\Phi = \frac{1-\sqrt{5}}{2} = -0.618\,033\,988\,749\,894\,9... \tag{4}$$

This other solution has the same decimal expansion as ϕ. An interesting property of the Golden ratio is that its reciprocal can be obtained by subtracting one, i.e.

$$\frac{1}{\phi} = \phi - 1 = 0.618\,033\,988\,749\,894\,9... \tag{5}$$

Preprints (www.preprints.org) | NOT PEER-REVIEWED | Posted: 16 August 2022 doi:10.20944/preprints202208.0293.v1

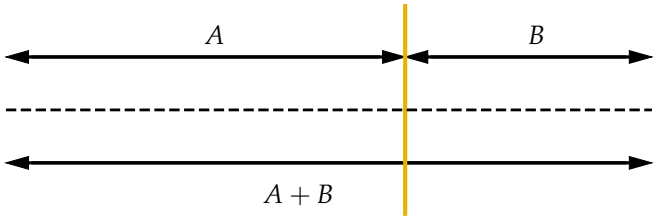

Figure 1. The Golden ratio may be defined as a cut to a line (dashed) into lengths A and B such that the ratio A/B is equal to the ratio $(A+B)/A$.

The Golden ratio seems to possess an almost mythical reputation compared to other numbers, as can be intuited from its name. Another name given to this number is the Divine Proportion, going back to the work of Italian mathematician Luca Pacioli, *Divina proportione*, in 1509. This reputation is fuelled by claims (often with dubious evidence) that ϕ explicitly occurs in certain famous architectural and artistic works, ranging from the Great Pyramid in Egypt and the Parthenon in Greece, to the paintings of Renaissance polymath Leonardo da Vinci (who illustrated Pacioli's work) [9].

Despite these misconceptions, ϕ has been found to legitimately occur in a diverse range of natural phenomena, at length scales varying from the atomic to those of galaxies. The purpose of this paper is to discuss a selection of these phenomena, and in doing so see how some of these may be linked. In Section 2, the mathematical properties of ϕ are explored further in the context of its irrationality. This is followed in Section 3 by a discussion of the various occurrences of ϕ in science, starting at the galactic length scale and proceeding to smaller lengths until reaching the atomic scale. Where appropriate, some of these occurrences of ϕ are explained in terms of the properties discussed in Section 2.

2. The 'Most Irrational' Number

The decimal expansion of ϕ never ends, and it never repeats. This is a consequence of the fact that ϕ is an *irrational* number, which means it cannot be expressed as a ratio of two integers. ϕ is sometimes referred to as the 'most irrational' number, a statement that strictly speaking makes no sense, as a number can either be rational (i.e. can be expressed as a ratio of two integers) or irrational (i.e. not rational). The reason for saying that ϕ is 'more irrational' than any other irrational number lies in the attempt to approximate it using rational numbers.

The approximation of irrational numbers using rational numbers is the subject of a branch of mathematics known as Diophantine approximation. Any irrational number can be approximated using a ratio of integers, for example, $\pi = 3.14159265...$, the ratio of a circle's diameter to its radius, can be approximated to two decimal places by the simple fraction $22/7$. Any real number (rational or irrational) may be expressed using a *continued fraction*,

$$a_0 + \cfrac{1}{a_1 + \cfrac{1}{a_2 + \cfrac{1}{a_3 + \cfrac{1}{\cdots}}}} \tag{6}$$

For a rational number, there are a finite number of integers, a_i, and so the continued fraction eventually ends. On the other hand, an irrational number has a never ending continued fraction expansion. An approximation to an irrational number can be found by finding a finite number of its a_i values. In the case of the Golden ratio, each of the a_i values are equal to one. The resulting approximations from this are ratios of numbers from the Fibonacci sequence. This famous sequence is defined by setting the first two terms both

Preprints (www.preprints.org) | NOT PEER-REVIEWED | Posted: 16 August 2022 doi:10.20944/preprints202208.0293.v1

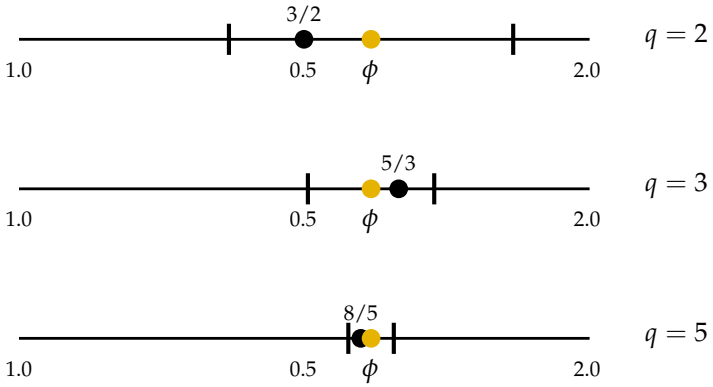

Figure 2. Approximation of the Golden ratio (gold) by ratios of successive Fibonacci numbers (black), for denominators $q = 2$ (top), $q = 3$ (middle) and $q = 5$ (bottom). As the denominator, q increases, the more accurate the approximation. The vertical lines in each case shows the upper bound for the deviation (from ϕ), as given by the right-hand side of Equation 9.

equal to one, and then each subsequent term is equal to the sum of the previous two. The first few Fibonacci numbers are,

$$1, 1, 2, 3, 5, 8, 13, 21, 34, 55, 89, ... \tag{7}$$

If a particular number from this sequence is divided by the previous term, the result is an approximation to ϕ. As the chosen Fibonacci number grows larger, the approximation to ϕ improves, as shown in Figure 2. For any irrational number, x, the continued fraction expansion may be used to obtain a sequence of rational approximations p/q (where p and q are respectively the numerator and denominator of the approximation). As q increases, the approximation becomes closer to the irrational number. To account for this when measuring how well the irrational number is approximated, one can multiply the difference between x and p/q by q^2. A result known as Dirichlet's approximation theorem shows that there exist infinitely many rational approximations that satisfy the inequality,

$$\left| x - \frac{p}{q} \right| < \frac{1}{q^2} \tag{8}$$

This provides an upper bound on how good the approximation can be. For any choice of x, the smallest possible value for this upper bound is given by Hurwitz's theorem [10],

$$\left| x - \frac{p}{q} \right| \leq \frac{1}{\sqrt{5}q^2} \tag{9}$$

In addition, equality holds only if $x = \phi$ (or any other number whose continued fraction expansion contains infinitely many 1's). Figure 3 shows how $q^2|\phi - p/q|$, (which may be interpreted as a relative error) varies as more terms in the continued fraction expansion are included. There is a rapid convergence towards $1/\sqrt{5} \approx 0.4472$. In other words, for most rational approximants of ϕ, the relative error term is close to the upper bound. Since for any other (non-equivalent) number, the upper bound is smaller, the rational approximants of the Golden ratio and its equivalents are worse than for any other number. It is for this reason that ϕ is often referred to as the 'most irrational' number.

3. The Golden Ratio in Nature

A wide variety of natural phenomena can be linked to the Golden ratio, and these occur on length scales ranging from the atomic to the astronomical. Here, some such

Preprints (www.preprints.org) | NOT PEER-REVIEWED | Posted: 16 August 2022 doi:10.20944/preprints202208.0293.v1

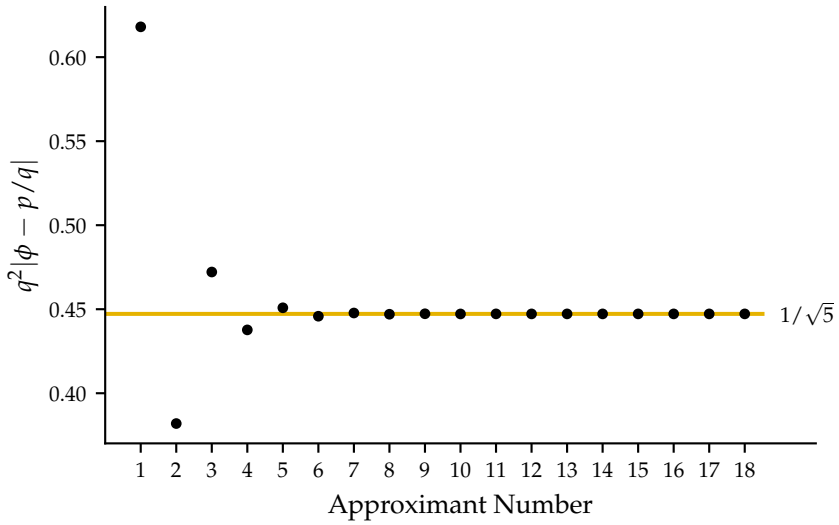

Figure 3. Relative error, $q^2|\phi - p/q|$, between the Golden ratio and its rational approximants, for the first 18 successive ratios of the Fibonacci sequence. There is rapid convergence to $1/\sqrt{5} \approx 0.4472$.

phenomena shall be explored, starting at the astronomical scale and progressing to smaller scales.

3.1. Spiral Galaxies

The largest length scale on which ϕ has been observed is that of galaxies, which comprise of billions of stars bound by gravity. Many galaxies are characterised by their visually striking spiral arms [11]. A commonly used mathematical model for these arms is the *logarithmic spiral*, shown in Figure 4, for which the shape remains the same as size increases due to a constant pitch angle. The equation for the logarithmic spiral is,

$$r = a \exp k\theta \tag{10}$$

where r and θ are plane polar coordinates, a is a constant parametrising size, and k is given by,

$$k = \tan(\chi) = \frac{1}{\tan(\psi)} \tag{11}$$

where pitch angle χ, and $\psi = \pi/2 - \chi$ are defined by Figure 4.

In studying a sample of 350 galaxies, it was found by Block and Fairall [12] that the pitch angle (in their paper, defined as the ψ angle) for galactic spiral arms averages at approximately $\psi = 73°$. The following year, Oldershaw [13] pointed out that this pitch angle yields a special logarithmic spiral known as the *Golden spiral*, whose radius grows by a factor of ϕ every time the turn angle, θ, increases by $\pi/2$. To show this, one can take Equation 10 for two points on the spiral, at radii r_1 and r_2, separated by a turn angle of $\pi/2$, to give,

$$r_1 = ae^{k\theta} \tag{12}$$

and

$$r_2 = \phi r_1 = ae^{k(\theta+\pi/2)} \tag{13}$$

Dividing Equation 13 by Equation 12 gives,

$$\phi = \frac{ae^{k(\theta+\pi/2)}}{ae^{k\theta}} = e^{k\times\pi/2} \tag{14}$$

Preprints (www.preprints.org) | NOT PEER-REVIEWED | Posted: 16 August 2022 doi:10.20944/preprints202208.0293.v1

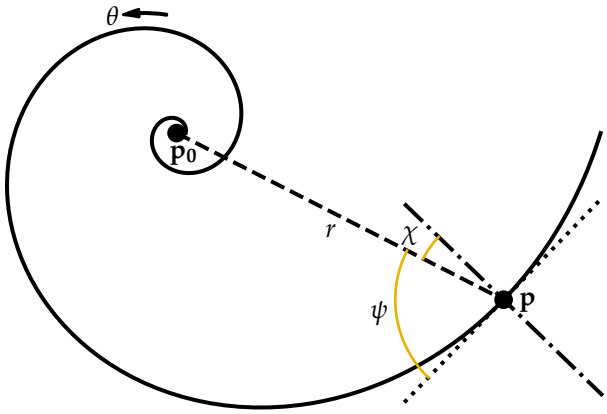

Figure 4. A point, $\mathbf{p}$, on any spiral can be described by its distance r from the centre point, $\mathbf{p_0}$, and a turn angle, θ. The tightness of a spiral at $\mathbf{p}$ is given by the pitch angle, χ, the angle between the centre-to-point vector (dashed line) and the normal to the spiral at $\mathbf{p}$ (dash-dotted line). Equivalently, the angle, ψ, to the tangent (dotted line) can be used instead, with $\psi + \chi = \pi/2$. For a logarithmic spiral, the pitch angle is constant over the whole spiral.

Taking the natural logarithm of both sides and rearranging gives,

$$k = \frac{2 \ln \phi}{\pi} \tag{15}$$

Substitution of this into Equation 11 gives,

$$\chi = \arctan\left(\frac{2 \ln \phi}{\pi}\right) = 0.29727... = 17.03239...^\circ \tag{16}$$

and therefore,

$$\psi = \pi/2 - \chi = 1.2735... = 72.9676...^\circ \tag{17}$$

Using galactic pitch angle data of 50 spiral galaxies, as measured by Savchenko and Reshetnikov [14], the pitch angle distribution shown in Figure 5 was generated. As can be seen, there is a peak for χ between 17° and 20°. The mean for this sample is $\bar{\chi} = 15.1520^\circ$ with a standard deviation of 3.6879, which just under a quarter of $\bar{\chi}$.

It should be noted that real spiral galaxies are not perfect logarithmic spirals. For real galaxies, the pitch angle can vary as radius increases. The work of Savchenko and Reshetnikov shows that galactic pitch angles (χ) decrease as r increases (the values used to plot the distribution are averages). Nevertheless, it is interesting that by approximating spiral galaxies using a simple geometric shape in the logarithmic spiral, the single parameter used to describe the shape appears to peak close to a value associated with the Golden spiral.

3.1.1. The Logarithmic Spiral

Other than galaxies, there exist a number of natural phenomena that are described by logarithmic spirals. Examples include the flight paths of insects [16] and birds [17], nautilus shells and tropical cyclones [18]. Such examples are often mentioned in connection with the Golden ratio (see for example, [5]). Quite often however, the spirals in question are not necessarily Golden [19]. The logarithmic spiral is so often connected with the Golden ratio because the Golden rectangle (i.e. a rectangle with Golden aspect ratio) can be used to construct an approximate logarithmic spiral, as shown in Figure 6. One can split a Golden rectangle by making a Golden cut along the long edge to form a square and a smaller Golden rectangle. This can then be performed on the smaller rectangle, and iterated to

Preprints (www.preprints.org) | NOT PEER-REVIEWED | Posted: 16 August 2022 doi:10.20944/preprints202208.0293.v1

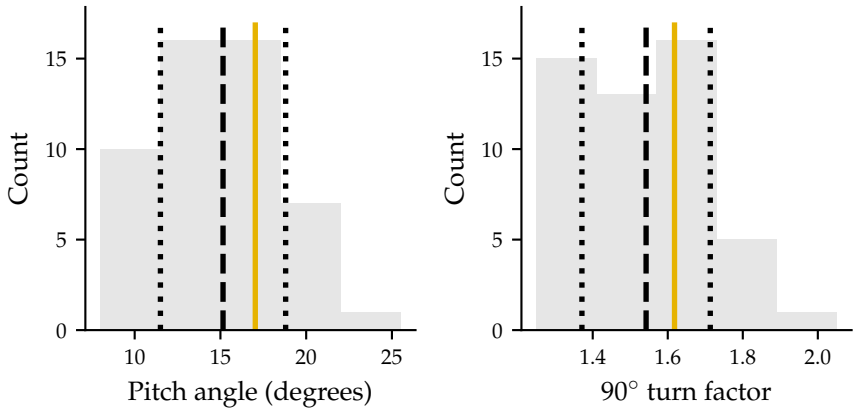

Figure 5. Distribution of pitch angles, χ (left) and corresponding turn factors over 90° (right), for a sample of 50 spiral galaxies. The gold solid line corresponds to the Golden spiral ($\chi = 17.03239...°$), while the dotted black line shows the mean of $15.1520° \pm 3.6879$ (with turn factor 1.5423 ± 0.1728). The dotted black lines indicate the range within one standard deviation from the mean. The galactic pitch angle data was taken from Table 1 in Reference [14]. The bin widths (3.5 and 0.16 respectively) were chosen based on Scott's rule [15].

generate yet smaller rectangles. An approximate logarithmic spiral can then be produced by drawing quarter circular arcs to connect opposite corners of the squares.

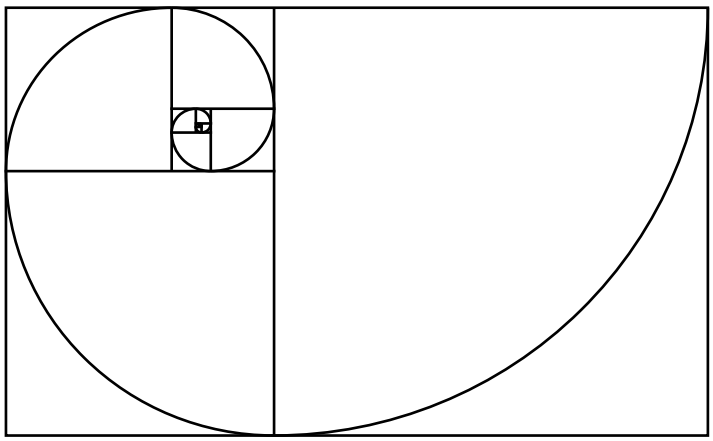

Figure 6. Approximation of the Golden spiral, using the Golden rectangle. The rectangle can be split into a square, and a smaller Golden rectangle. Then circular arc lengths can be drawn across the squares, with radius equal to the square length. This means each arc has a different radius, thus the resulting spiral is not logarithmic.

While the above example of spiral galaxies does appear to distribute about a pitch angle close to that of the Golden spiral, a case that does not is that of the nautilus shell [20–22]. Despite this, the image of the nautilus shell has become synonymous with the Golden ratio, as evidenced by such an image being featured on the front cover of many books on the Golden ratio (for example, References [3–7]).

The case of the nautilus shell is a cautionary example that shows the need to be careful when encountering claims that the Golden ratio appears in some phenomenon. On the one hand, there may be an element of misunderstanding, such as confusion over the Golden spiral and the more general logarithmic spiral. On the other hand, too much scepticism could lead to legitimate occurrences of ϕ in nature being overlooked.

Preprints (www.preprints.org) | NOT PEER-REVIEWED | Posted: 16 August 2022 doi:10.20944/preprints202208.0293.v1

3.2. Variable Stars

One such legitimate appearance of ϕ in nature may be found in a particular class of variable star. Many stars, such as the Sun, have a luminosity that remains roughly the same over time. Some stars however, have a variable luminosity, caused by periodic changes in pressure. One such class of star are the *RR Lyrae variables* (named after the variable star RR Lyrae), which are useful to astronomers as standard candles. Some of these variable stars pulsate with multiple frequencies. Using data from the Kepler space telescope, Lindner et al. studied four RR Lyrae variable stars with pulsation frequencies found to be in the Golden ratio [23]. It has been noted that many variable stars of multiple frequencies have frequency ratios between 0.6 and 0.64 [24]. Lindner et al. found that these stars exhibit 'strange nonchaotic dynamics', meaning that they have fractal behaviour without showing chaotic behaviour. This is a highly non-trivial observation since fractal dynamics is often associated with chaos. These stars are the first discovered natural phenomena to show this form of dynamics, which was first discussed by Grebogi et al. in 1984 [25]. Other variable stars, with commensurate pulsation frequencies were also studied, and these did not exhibit strange nonchaotic behaviour. Studies of simple non-linear systems (crudely modelling a variable star) [26] also revealed Golden behaviour. This suggests that the observed variable star behaviour may be a universal feature of such non-linear systems.

3.3. Planetary Orbits

Focusing now on the orbits of planets around a star, an interesting manifestation of Fibonacci numbers and the Golden ratio may be found in the Solar System. It has been noted that the mean distances of the planets from the Sun approximately relate to each other according to the Golden ratio [27,28]. The ratios of successive orbits periods have been found to be preferentially closer to Fibonacci ratios than to other fractions; not only for planets in the Solar System, but also for satellites of the gas giants and even in exoplanetary systems [29].

Dynamics simulations can be used to verify that the orbital periods of the planets (the time taken for each planet to complete one orbit of the Sun) relate to each other according to Fibonacci numbers. In such a simulation [1], the Sun and eight planets interacted *via* gravity, and the simulated time was 1630×365.25 days, which is approximately 1630 Earth years. Inspired by Reference [28], this time was chosen as it is about the time taken for Mercury to complete 6765 orbits, with 6765 being the twentieth Fibonacci number. The number of orbits made by each planet in this time was recorded from the simulation, the results of which are shown in Table 1. Each planet completes a number of orbits approximately equal to a Fibonacci number, with the exception of Mars and Neptune, which nonetheless do complete a multiple of a Fibonacci number of orbits.

Planet	Number of orbits	Fibonacci number	Error (%)
Mercury	6960.37	6765	2.89
Venus	2655.04	2584	2.75
Earth	1627.75	1597	1.93
Mars	870.59	144×6	0.76
Jupiter	136.11	144	5.48
Saturn	54.03	55	1.77
Uranus	19.56	21	6.84
Neptune	10.20	5×2	1.98

Table 1. Number of orbits completed by each planet in a Molecular dynamics simulation with a simulated time of 1630 Earth years (i.e. 1630×365.25 days). These values are compared to Fibonacci numbers, with percentage errors given to two decimal places.

[1] A Python implementation of this simulation is available at http://doi.org/10.17639/nott.7230.

Preprints (www.preprints.org) | NOT PEER-REVIEWED | Posted: 16 August 2022 doi:10.20944/preprints202208.0293.v1

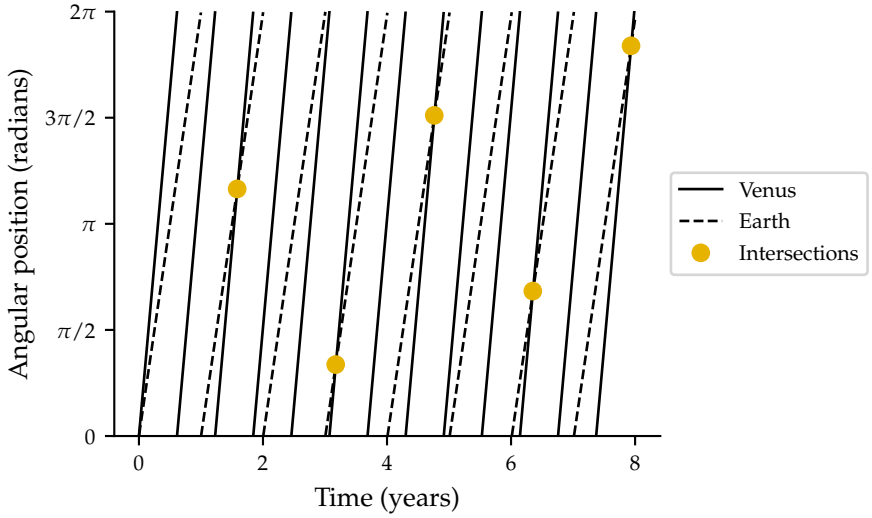

Figure 7. Synodic conjunctions of Venus (solid lines) and Earth (dashed lines). Within eight Earth years, the two planets are co-linear five times (gold circles).

This shows a clear link between planetary orbits and the Fibonacci sequence, therefore suggesting that the ratios between the orbital periods are close to multiples of the Golden ratio. In particular, ϕ can be most clearly found when considering the orbits of Earth and Venus. Starting from a configuration where the Sun, the Earth and Venus are co-linear, after eight Earth years this co-linear state (known as a *synodic conjunction*) occurs five times (with 8/5 being a Fibonacci ratio), as shown by the intersections in Figure 7, which plots the angular position in the orbit of the two planets against time. Furthermore, if the number of orbits made by Venus is plotted against the number of Earth orbits as in Figure 8, the relationship is linear for long times (i.e. over multiple years) with Fibonacci numbers plotted against the previous terms in agreement with this line. Performing linear regression on this data yields a slope of $1.631 \approx \phi$.

3.4. The KAM Theorem

An explanation of why the ratio of planetary orbital periods coincides with ϕ is presented by the KAM (Kolmogorov–Arnold–Moser) theorem [30,31]. This theorem applies to integrable (i.e. the equations of motion can be analytically solved) dynamical systems that are subject to a small non-linear perturbation. For example, the motion of a single planet around a star due to gravitation is an integrable system, while the effect of an additional planet is a perturbation. The evolution of a dynamical system can be represented as a trajectory in *phase space*, the space of all possible states of the system. For any integrable system, this trajectory is confined to the surface of an n-dimensional torus embedded in the $2n$-dimensional phase space (where n is the number of independent degrees of freedom of the system) [32]. These surfaces are known as *invariant tori* because a trajectory that begins on such a surface remains on the surface for all values of time. The exact torus on which the trajectory resides is determined by the initial conditions of the system. Given that the phase space trajectory of an integrable system lies on an n-dimensional invariant torus, the dynamics of the system can be described by the combined effect of the n periodic motions along each independent direction of the torus. Thus, for $i = 1, ..., n$, there are n natural frequencies, ω_i on the torus. The ratios, $\omega_i / omega_j$, are called the *winding numbers* of the torus. In the case where each winding number is rational, the trajectory is periodic, whereas if any winding numbers are irrational, then the trajectory eventually covers every point of the torus - in which case the trajectory is *quasiperiodic*.

According to the KAM theorem, under a small perturbation to an integrable system, some of these tori are deformed but still remain as invariant surfaces, while others are

Preprints (www.preprints.org) | NOT PEER-REVIEWED | Posted: 16 August 2022 doi:10.20944/preprints202208.0293.v1

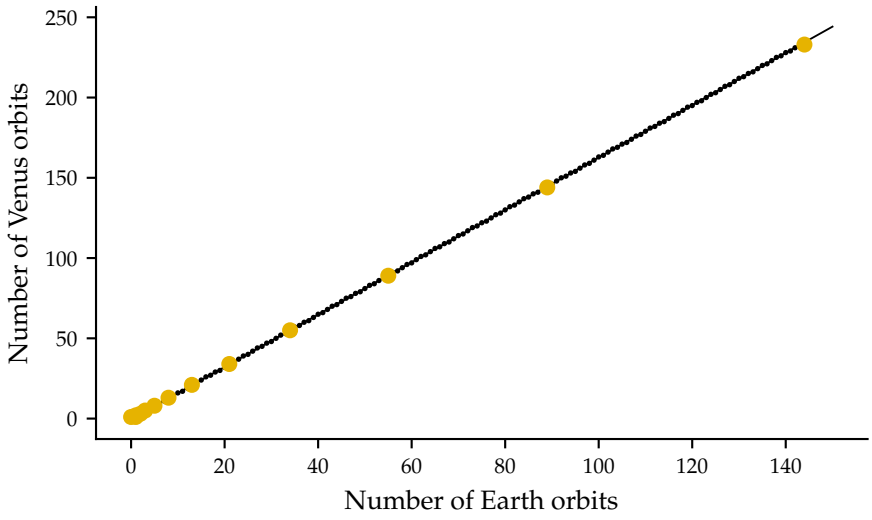

Figure 8. Number of orbits completed by Venus against the number of Earth orbits as calculated from the dynamics simulation (black points). The gold circles show the Fibonacci numbers against the previous term. A linear fit to this data has slope 1.631.

destroyed and so the trajectory is no longer restricted. A stronger perturbation to the system results in the destruction of more invariant tori. The surviving tori have frequencies whose ratios are 'sufficiently irrational'. A consequence of this is that dynamical systems with frequencies of an irrational ratio are more resilient to perturbations [33]. Since the Golden ratio is the 'most irrational' number, a Golden frequency ratio provides the most resistance to perturbations. Thus, in the case of the Solar System, having orbital periods related by ϕ maximises stability.

3.5. Phyllotaxis

Observations of ϕ are not restricted to only celestial objects. A commonly noted Earthly case is that of phyllotaxis [34–36], the arrangement of leaves on a stem, which form spiral patterns. In such spirals, the rotational angle around the stem from leaf to leaf is approximately $2\pi/\phi \approx 222.49°$, the angle that divides the circumference of a circle into the Golden ratio. The reason for this is that the 'maximally irrational' property of ϕ provides the least chances for leaves to be positioned directly above each other, and thus each leaf receives the maximum possible amount of sunlight.

A mathematically rigorous explanation for why the Golden angle is optimal is offered by Bergeron and Reutenauer [37]. In their paper, a simple model of 'buds' growing along a helix on a cylindrical 'plant' is studied. Around each bud, a disk is placed with diameter such that no overlap occurs. Then it is shown that a quantity representing the 'capacity' of the plant (i.e. the ability for the plant to grow the most number of buds using minimal disk area) is optimised when the rotational angle is Golden. The proof of this makes use of the irrationality of ϕ in the sense discussed above (See Section 2).

3.6. The Ultimatum Game

In game theory, the branch of mathematics devoted to understanding strategic decision making when two 'players' interact, the Golden ratio appears in the 'ultimatum game', first described by Güth et al. [38]. In this game, one player has a set amount of some resource (money, for example), and must offer a share of this to a second player. If the second player accepts, then the resource is divided according to the offer. If they reject the offer, then both players leave empty handed. One might think that the best possible strategy for the first player is to make the smallest possible (non-zero) offer, while the second player's best strategy is to accept this. However, in practice, this is not found to be the actual outcome.

Preprints (www.preprints.org) | NOT PEER-REVIEWED | Posted: 16 August 2022 doi:10.20944/preprints202208.0293.v1

The most likely accepted offers tend to be around 40% [39]. It has been suggested that the solution to the ultimatum game is to make an offer such that the proportion of the second player's share to the first player's equals that of the first player to the whole, i.e. the Golden section. This solution could be interpreted as the fairest possible trade-off given an asymmetric situation. The ultimatum game has been applied to a wide range of situations, including that of human walking [8]. In this case, there are two phases: the stance (when both feet are on the ground) and swing (when a foot leaves the ground). The most common ratio between the times spent in each of these phases was found by Iosa *et al.* to be Golden. From the game theory perspective, the Golden ratio provides the optimal compromise between continued motion and stability of the walker.

3.7. The Human Body

Knowing that the Golden ratio plays a role in human walking, one might ask whether it also appears in the human body? The answer to this question is that is does, and in a variety of situations including the heart as well as the brain.

3.7.1. The Heart

The work of Henein *et al.* [40] shows three cases of ϕ present in the human heart. Their work used images obtained by ultrasound, as well as Firstly, it was found that vertical and transverse measurements of the left ventricle (one of the chambers of the heart) are in the Golden ratio. Secondly, the annulus dimensions in the mitral valve (located between the left ventricle and left atrium) were also found to be in the Golden ratio. Thirdly, the angle between the right ventricular inlet axis and the outflow tract axis was found to be close to the Golden angle, 137.5°. For all three of these measurements, there was an observed deviation from ϕ when the heart was not healthy. This means that such measurements could be used as a way to identify when the heart deviates from normality.

3.7.2. The Brain

A recent discovery is that ϕ occurs in the dimensions of the human skull. The work of Tamargo and Pindrik [41] took computerised axial tomography (CAT) scanned images of human skulls and considered three points; the *nasion* (where the frontal bone meets the nasal bones), the *inion* (a protuberance at the back of the skull) and the *bregma* (a point at the top of the skull where the frontal and parietal lobes meet). Taking the arc joining the nasion and inion, and dividing it into two sections separated by the bregma, Tamargo and Pindrik found that the resulting sections are Golden, i.e. the bregma makes a Golden cut to this arc. They also found that the equivalent skull dimensions of some other mammals, such as monkeys, rabbits, dogs, lions and tigers, have differing ratios. Furthermore, these ratios appear to approach ϕ as the species becomes more sophisticated.

3.8. Proteins and Amino Acids

With the ubiquity of ϕ in various organs of the human body, it seems natural to ask whether ϕ appears at smaller biological scales. Recently, the Golden ratio has also been observed at the nanometre scale [42], in the shape of proteins, macromolecules which play a vital role in our existence. The distribution of protein aspect ratios, obtained using calliper measurements from the Protein Data Bank (PDB), are shown in Figure 9. There are two peaks in this distribution, one for prolate (cigar shaped) proteins, and one for oblate (frisbee shaped) proteins. The mode aspect ratio in the prolate case is close to the Golden ratio, while the peak oblate shape is close to its reciprocal.

It was also observed that the amino acids that comprise proteins have aspect ratios which distribute to a value near the Golden ratio. For each residue in the protein dataset (approximately 13 million amino acids), the spheroid of equivalent steric volume to the side chain was calculated. This gives a distribution of aspect ratios for each of the 20 types of amino acid found in proteins. The average aspect ratio (the ratio between the spheroid major axis, a, and minor axis b) for each amino acid type (not including glycine, whose side

Preprints (www.preprints.org) | NOT PEER-REVIEWED | Posted: 16 August 2022 doi:10.20944/preprints202208.0293.v1

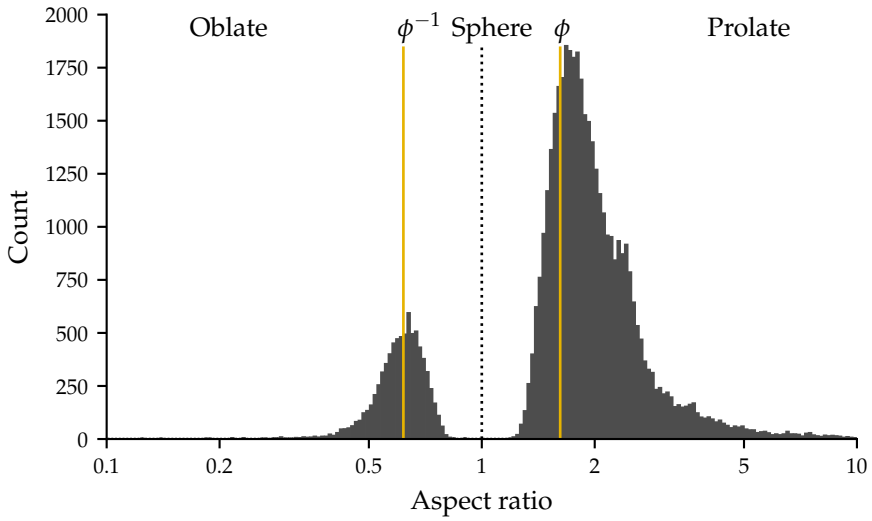

Figure 9. Distribution of aspect ratios of proteins, as obtained by calliper measurements. The distributions for oblate (aspect ratio < 1) and prolate (aspect ratio > 1) proteins peak near aspect ratios of ϕ^{-1} and ϕ, respectively (gold lines).

chain consists of a single hydrogen atom) is shown in Figure 10. It can be seen that the ratios a/b and $(a+b)/a$ distribute around a value close to ϕ. It can be noted that the average values of $(a+b)/a$ and a/b (1.6120 and 1.6808) are quite close to each other, suggesting that the average shape of amino acids is close to Golden. Interestingly, when taking into account the number of residues of each type in the protein data, the average aspect ratio drops to about 1.5152 (black line in Figure 10). This can be explained by noting that the three most commonly occurring amino acid types in the protein dataset, alanine (ALA), leucine (LEU) and valine (VAL), have relatively low aspect ratios (all below 1.6).

It is an interesting observation that amino acids in proteins have a shape similar to that of the proteins they make up, and that this common aspect ratio coincides with ϕ, which is itself defined using the idea of self-similarity.

3.9. Penrose Tilings and Quasicrystals

In addition to proteins, another example of how atoms can assemble in a self-similar fashion is that of *quasicrystals*, structures that are ordered in space but that are not periodic. A *crystal* is an ordered arrangement of points, usually with a regularly repeated (i.e. periodic) pattern. A mathematical result known as the *crystallographic restriction theorem* states that the only allowed rotational symmetries for a crystal are 2, 3, 4 and 6-fold. In other words, a periodic tiling using one of these symmetries can be used to completely fill space. This does not apply to 5-fold, or x-fold (where $x > 6$) symmetry, meaning for example, that it is not possible to tile two-dimensional space using regular pentagons. In the geometry of the regular pentagon, the Golden ratio appears. As pictured in Figure 11, the diagonal length divided by the side length equals ϕ. Thus, the Golden ratio may be associated with five-fold symmetry in a similar way to how the number $\pi = 3.14159...$ is associated with circular symmetry.

It was discovered by Penrose that two-dimensional space can in fact be tiled by using a pair of shapes derived from the pentagon [43]. An example of such a tiling, where each tile is one of two types of rhombus, is shown in Figure 12. The Penrose tiling has the property of not being periodic, but yet is self-similar in that finite patches of the tiling are repeated infinitely many times. Also, it is possible to transform a Penrose tiling into another equivalent tiling by applying a particular set of substitution rules on the tiles. The Penrose tiling also exhibits multiple instances of the Golden ratio, as might be expected due to its

Preprints (www.preprints.org) | NOT PEER-REVIEWED | Posted: 16 August 2022 doi:10.20944/preprints202208.0293.v1

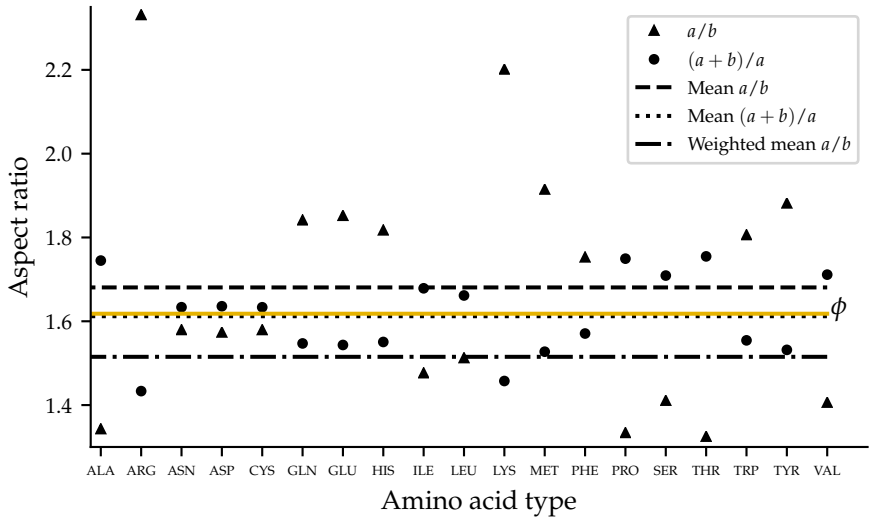

Figure 10. Average aspect ratios of 19 amino acid types (excluding glycine), as calculated from spheroids of equivalent steric volume to amino acid side chains in each protein. The triangles show the ratio a/b, while the circles show the ratio $(a+b)/a$. The dashed and dotted lines show the average values of the triangles (1.6808) and circles (1.6120) respectively, while the gold solid line shows the Golden ratio. Also shown, by the dash-dotted line, is the average aspect ratio, a/b, weighted by the frequency of each residue in the protein data (1.5152).

five-fold symmetry. The Golden ratio is prominent in the geometry of the tiles themselves, and in the limit of infinitely many tiles, the ratio of wide to thin rhombi is ϕ.

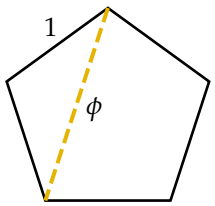

Figure 11. The ratio between the diagonal (dashed gold line) and the side length of a regular pentagon is the Golden ratio.

To see how the Golden ratio appears in the Penrose tiling, it is useful to consider a one-dimensional example of a 'tiling', based on the Fibonacci sequence. This example may be constructed by first taking a square lattice in two dimensions, and defining a strip as shown in Figure 13, such that its slope is $1/\phi$. If the strip is defined by taking a unit square and moving it along this direction, then the projections of the points within the strip onto the axis parallel to the slope define a series of line segments. It can be seen in Figure 13 that the line segments have one of two lengths, one short and one long. The ratio between these lengths is itself Golden, and the sequence of long and short line segments is equivalent to the Fibonacci sequence. The Penrose tiling can be interpreted as a superposition of five sets of Fibonacci lattices. It was found by Ammann [44,45] that the rhombus matching rules can be formulated by drawing straight lines on the tiles, such that the lines continue when two tiles are placed edge to edge. Figure 14 shows these Ammann lines overlaid on a Penrose tiling. There are five sets of parallel lines, and for each such set of lines, there are two separation lengths. These sets of lines are themselves Fibonacci lattices. The Penrose tiling could thus be viewed as a two-dimensional generalisation of the Fibonacci lattice.

In three dimensions, a forbidden symmetry is that of the icosahedron, a twenty faced regular polyhedron whose geometry features five-fold symmetry and the Golden

Preprints (www.preprints.org) | NOT PEER-REVIEWED | Posted: 16 August 2022 doi:10.20944/preprints202208.0293.v1

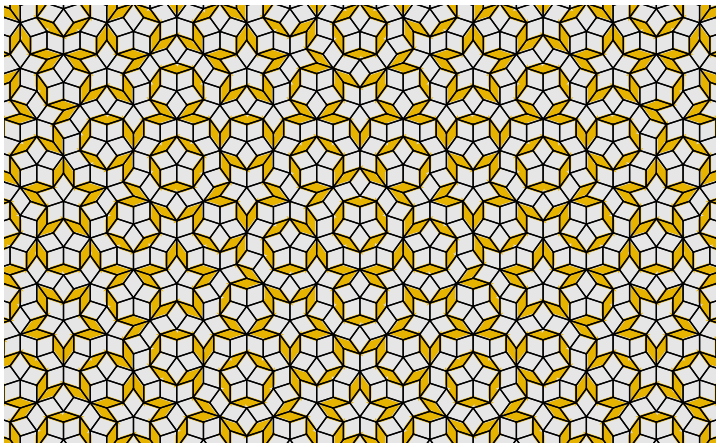

Figure 12. Finite patch of a Penrose tiling of the plane, using two types of rhombus derived from the pentagon. The thin tiles (gold) have internal angles of 36° and 144°, while the wide tiles (silver) have angles 72° and 108°. In the infinite tiling, the ratio of wide to thin tiles is Golden.

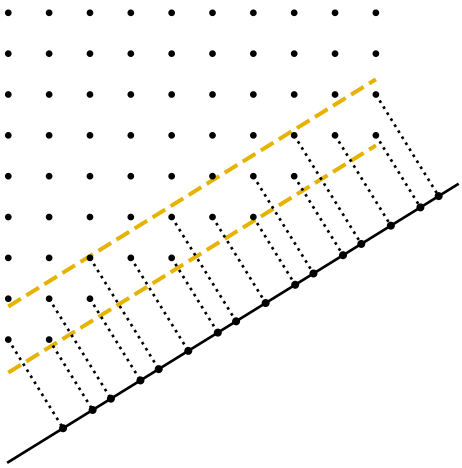

Figure 13. Generation of a Fibonacci chain by projection from a two dimensional lattice. A strip (between the two gold dashed lines) of slope $1/\phi$ is defined by translating a unit square along this direction, and all lattice points within this strip are found. These points are then projected onto an axis of the same slope (solid black line) and this forms a chain of long and short length segments, which behaves according to the Fibonacci sequence.

Preprints (www.preprints.org) | NOT PEER-REVIEWED | Posted: 16 August 2022 doi:10.20944/preprints202208.0293.v1

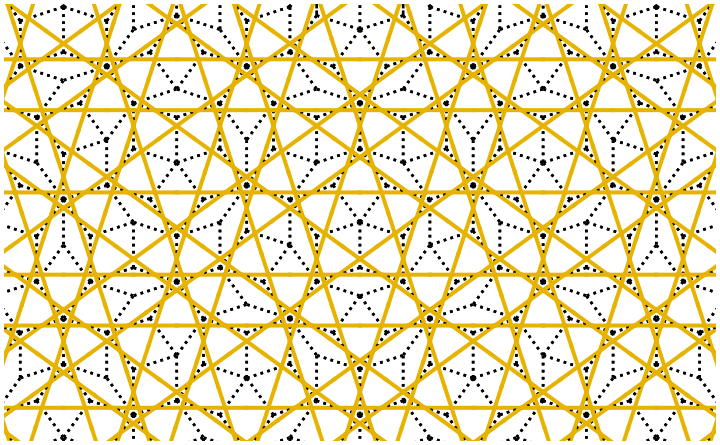

Figure 14. Penrose tiling (black dotted rhombi) with overlaid Ammann lines (gold solid lines). These lines provide a means of specifying matching rules between tiles, with the rule being that the lines must remain continuous. The set of Ammann lines in a full Penrose tiling is equivalent to a set of five overlapping Fibonacci chains.

ratio. The Nobel prize winning discovery by Shechtman of icosahedral symmetry in an aluminium-manganese alloy [46], shows that the crystallographic restriction theorem can be violated by real materials. This shows that a 'crystal' structure can be ordered, in that the positions of the tiles are governed by some mathematical prescription, and yet not be periodic. Such structures are known as quasicrystals [47]. There are two types of known thermodynamically stable quasicrystal in three dimensions: polygonal and icosahedral. Polygonal quasicrystals have an axis of either 8, 10 or 12-fold symmetry, with the structure being aperiodic in planes normal to this axis and periodic along it. Icosahedral quasicrystals on the other hand, are aperiodic along all three dimensions. The work of Steinhardt *et al.* [48,49] considers the icosahedral quasicrystal as the three-dimensional analogue of the Penrose tiling. Icosahedral quasicrystals have been discovered as naturally occurring in samples from the Koryak Mountains in Siberia [50–52]. Given the presence of the Golden ratio in the geometry of the icosahedron, it is an interesting observation that this symmetry is the only way to produce a quasicrystal that satisfies quasi-periodicity along all three dimensions, and that it is found in the only known natural quasicrystals.

3.10. Atomic Bond Lengths

While proteins, amino acids and quasicrystals show examples of how many atoms can arrange themselves with geometry described by ϕ, the Golden ratio also appears when considering the bonds between pairs of atoms, and can be used as a simple model to predict bond lengths. Using density functional methods, Suresh and Koga obtained a value of 0.0327 nm for the hydrogen-carbon bond lengths in methane [53]. The work of Heyrovska [54,55] was motivated by the fact that this value is close to the Bohr radius, the most probable ground state distance between the proton and electron in the hydrogen atom (0.0529 nm), divided by the Golden ratio. This work shows that the Bohr radius can be divided into Golden sections, a_e and a_p, corresponding to the electron and proton respectively. The ionisation energy for hydrogen in the ground state (i.e. the energy required to separate the electron and proton) can then be written as a difference of two terms based on these distances. This idea has been extended to the case of a covalent bond between two identical atoms. For atoms of type A, the length of such a bond, $d(\mathrm{AA})$, can be considered the sum of two radii, $d(\mathrm{A}^+)$ and $d(\mathrm{A}^-)$, defined by a Golden cut. Given the covalent bond length for a pair of identical atoms, the values of $d(\mathrm{A}^+)$ and $d(\mathrm{A}^-)$ may be calculated for the atom of type A. These values can then be used, as in Reference [54], to predict the bond length between two dissimilar atoms.

Preprints (www.preprints.org) | NOT PEER-REVIEWED | Posted: 16 August 2022 doi:10.20944/preprints202208.0293.v1

3.11. Black Holes, Quantum Gravity and E8

The two most successful physics theories of the twentieth century are general relativity and quantum mechanics. The former describes gravity and the universe at large scales, while the latter describes the universe at small scales using electromagnetism, the strong nuclear and weak nuclear forces. However, the two theories are notorious for their mutual incompatibility with each other. An example that invokes both theories is that of black holes, which have sufficiently strong gravity that even light cannot escape, and are so compact that quantum effects are important. The study of black holes has revealed multiple instances of the Golden ratio, two of which are discussed here.

A well known example is that of the specific heat capacity of a black hole. Specific heat capacity is defined as the amount of energy that must be added to a unit mass of some object in order to raise its temperature by one unit. Due to a result known as the virial theorem, self-gravitating objects, such as stars, have a negative specific heat, i.e. they become hotter when energy is removed [56]. This happens because as energy is removed, the star contracts and so its constituent particles speed up, increasing the temperature. The same is true of a Schwarzschild black hole, which is a spherically symmetric, non-rotating black hole with zero net charge. When considering a black hole that is rotating, the specific heat capacity can be positive or negative, depending on the angular momentum. It was found by Davies [57] that the transition between negative and positive occurs when the black hole satisfies (using units in which the speed of light and the gravitational constant equal unity),

$$\frac{J^2}{M^4} = \sqrt{2\sqrt{3} - 3} \approx 0.464 \tag{18}$$

where M is the mass of the black hole, and J is its angular momentum. Interestingly, a later paper by Davies [58] showed that the same ratio, J^2/M^4 equals the inverse Golden ratio, $(1 - \sqrt{5})/2$. This latter result has been found to be true, if the ratio of angular momentum and mass is held constant [59].

While the heat capacity example seems physically unlikely (as there is no reason to expect that the angular momentum to mass ratio of a black hole to remain constant), Cruz et al. [60] showed that ϕ also appears in black hole physics when considering the metric (a mathematical object describing spacetime curvature) of Schwarzschild-Kottler black holes. In particular, ϕ appears when considering the null geodesics (i.e. the paths taken by photons) of this metric.

Given the appearance in ϕ in black holes, one might question whether it also appears in theories attempting to unify general relativity and quantum theory. Some such attempts involve a mathematical structure known as 'E8' [61–63], in which ϕ may also be found [64]. One way to think of the E8 structure is as a lattice of points, corresponding to the densest way to pack 'spheres' in eight-dimensional space [65]. Evidence of an E8 governed phenomenon in nature was found by Coldea *et al.*, with the Golden ratio appearing in a low temperature one-dimensional magnet known as an Ising chain, formed by cobalt niobate [66]. When a critical magnetic field is applied perpendicular to the compound, the spin of each cobalt atom enters a quantum superposition of the up and down states. According to theoretical predictions, in the vicinity of the critical field, the two lightest particles of the chain should have masses in the Golden ratio [67]. In the cobalt niobate experiment, neutron scattering revealed two peaks in energy, interpreted as the two lightest particles of the Ising chain. As the applied field was increased, their ratio approached ϕ. As pointed out by Affleck [68], the observation of ϕ suggests that E8 underlies this system.

While the cobalt niobate experiment is currently the only case of an observed E8 governed system, it shows that the Golden ratio can be found at the quantum scale. The examples discussed above show that there is a tendency for ϕ to appear at all length scales, sometimes in surprising places. This tendency for the Golden ratio to appear in such a wide variety of phenomena has even led to suggestions that the Golden ratio is a fundamental constant of nature [69,70].

4. Conclusions

A remarkable number of apparently disparate natural phenomena can be linked to the Golden ratio, and occurrences of this number may be found at multiple length scales, ranging from the galactic to the atomic. Some of these instances; such as planetary orbits, phyllotaxis and quasicrystals, stem from the fact that the Golden ratio is, in the sense of Hurwitz's theorem, the most difficult number to approximate using rational quotients. In such cases, the Golden ratio manifests itself through its rational approximants, given by the ratios of successive Fibonacci numbers. In other cases; including spiral galaxy pitch angles, protein and amino acid shape, atomic bond lengths and black holes, the observations or calculations resulting in the Golden ratio appear coincidental, but may also indicate that some deeper, as yet unknown, explanation exists.

The propensity of this number to appear in unexpected places does however, sometimes lead to misconceptions, such as the idea that the nautilus shell and hurricanes are governed by the Golden spiral. Nevertheless, in exploring just one single number, one may encounter a plethora of fascinating topics from a variety of disciplines. Whenever the Golden ratio (or a nearby value) is encountered in science, there is an exciting opportunity for scientific, philosophical and artistic investigations.

Author Contributions: Conceptualization, CRM; methodology, CRM; software, CRM; investigation, CRM; writing—original draft preparation, CRM; writing—review and editing, CRM and PMW; supervision, PMW; All authors have read and agreed to the published version of the manuscript.

Funding: This work was supported by the Engineering and Physical Sciences Research Council DTP funding (EP/M50810X/1) to the University of Nottingham, and the University of Nottingham, via a PhD studentship to CRM.

Data Availability Statement: Python code implementing the simulation discussed in Section 3.3 is openly available in the Nottingham Research Data Management Repository at http://doi.org/10.17639/nott.7230.

Acknowledgments: CRM acknowledges the help and support of Phil Williams, School of Pharmacy, University of Nottingham.

Conflicts of Interest: The authors declare no conflict of interest.

Abbreviations

The following abbreviations are used in this manuscript:

KAM	Kolmogorov–Arnold–Moser
CAT	Computerized axial tomography
PDB	Protein data bank

References

1. Thompson, D.W. *On Growth and Form*; Cambridge University Press: Cambridge, 2014. Edited by J. T. Bonner.
2. Huntley, H.E. *The Divine Proportion: A Study in Mathematical Beauty*; Dover Publications, Inc.: New York, 1970.
3. Ghyka, M. *The Geometry of Art and Life*; Dover Publications, Inc.: New York, 1977.
4. Dunlap, R.A. *The Golden Ratio and Fibonacci Numbers*; World Scientific: Singapore, 1997.
5. Livio, M. *The Golden Ratio: The Story of Phi, the World's Most Astonishing Number*; Broadway Books: New York, 2003.
6. Olsen, S. *The Golden Section: Nature's Greatest Secret*; Wooden Books: Glastonbury, 2006.
7. Corbalán, F. *The Golden Ratio: The mathematical language of beauty*; National Geographic: Villatuerta, 2016.
8. Iosa, M.; Morone, G.; Paolucci, S. Golden Gait: An Optimization Theory Perspective on Human and Humanoid Walking. *Front. Neurorobot.* **2017**, *11*. https://doi.org/10.3389/fnbot.2017.00069.
9. Markowsky, G. Misconceptions about the Golden Ratio. *Coll. Math. J* **1992**, *23*, 2–19. https://doi.org/10.1080/07468342.1992.11973428.
10. Benito, M.; Escribano, J.J. An Easy Proof of Hurwitz's Theorem. *Amer. Math. Monthly* **2002**, *109*, 916. https://doi.org/10.2307/3072459.
11. Sparke, L.S.; Gallagher, J.S. *Galaxies in the Universe: An Introduction, 2nd Edition*; Cambridge University Press: Cambridge, 2007.
12. Block, D.L.; Fairall, A.P. Some Comments on the Pitch Angle in Spiral Structure. *Mon. Notes Astron. Soc. S. Afr.* **1981**, *40*, 43.

13. Oldershaw, R.L. The Preferred Pitch Angle of Spiral Galaxies; Mathematical and Physical Implications. *Mon. Notes Astron. Soc. S. Afr.* **1982**, *41*, 42. Provided by the SAO/NASA Astrophysics Data System.
14. Savchenko, S.S.; Reshetnikov, V.P. Pitch angle variations in spiral galaxies. *Mon. Not. R. Astron. Soc.* **2013**, *436*, 1074–1083. https://doi.org/10.1093/mnras/stt1627.
15. Scott, D.W. On optimal and data-based histograms. *Biometrika* **1979**, *66*, 605–610. https://doi.org/10.1093/biomet/66.3.605.
16. Boyadzhiev, K.N. Spirals and Conchospirals in the Flight of Insects. *Coll. Math. J* **1999**, *30*, 23–31. https://doi.org/10.1080/07468342.1999.11974025.
17. Tucker, V.A. The deep fovea, sideways vision and spiral flight paths in raptors. *J. Exp. Biol.* **2000**, *203*, 3745–3754. https://doi.org/10.1242/jeb.203.24.3745.
18. Moon, Y.; Nolan, D.S. Spiral Rainbands in a Numerical Simulation of Hurricane Bill (2009). Part I: Structures and Comparisons to Observations. *J. Atmos. Sci* **2015**, *72*, 164–190. https://doi.org/10.1175/jas-d-14-0058.1.
19. Sharp, J. Spirals and the Golden Section. *Nexus Netw. J.* **2002**, *4*, 59–82. https://doi.org/10.1007/s00004-001-0005-x.
20. Falbo, C. The Golden Ratio—A Contrary Viewpoint. *Coll. Math. J* **2005**, *36*, 123–134. https://doi.org/10.1080/07468342.2005.11922119.
21. Gailiunas, P. The Golden Spiral: The Genesis of a Misunderstanding. In Proceedings of Bridges 2015: Mathematics, Music, Art, Architecture, Culture; Delp, K.; Kaplan, C.S.; McKenna, D.; Sarhangi, R., Eds.; Tessellations Publishing: Phoenix, Arizona, 2015; pp. 159–166.
22. Bartlett, C. Nautilus Spirals and the Meta-Golden Ratio Chi. *Nexus Netw. J.* **2019**, *21*, 641–656. https://doi.org/10.1007/s00004-018-0419-3.
23. Lindner, J.F.; Kohar, V.; Kia, B.; Hippke, M.; Learned, J.G.; Ditto, W.L. Strange Nonchaotic Stars. *Phys. Rev. Lett.* **2015**, *114*. https://doi.org/10.1103/physrevlett.114.054101.
24. Moskalik, P. Multi-mode oscillations in classical Cepheids and RR Lyrae-type stars. *Proc. Int. Astron. Union* **2013**, *9*, 249–256. https://doi.org/10.1017/s1743921313014403.
25. Grebogi, C.; Ott, E.; Pelikan, S.; Yorke, J.A. Strange attractors that are not chaotic. *Physica D* **1984**, *13*, 261–268. https://doi.org/10.1016/0167-2789(84)90282-3.
26. Lindner, J.F.; Kohar, V.; Kia, B.; Hippke, M.; Learned, J.G.; Ditto, W.L. Simple nonlinear models suggest variable star universality. *Physica D* **2016**, *316*, 16–22. https://doi.org/10.1016/j.physd.2015.10.006.
27. Lombardi, O.W.; Lombardi, M.A. The Golden mean in the solar-system. *Fibonacci Q.* **1984**, *22*, 70–75.
28. Tattersall, R. A remarkable discovery: All Solar system periods fit the Fibonacci series and the Golden Ratio. Why Phi?, 2013. Available at: https://tallbloke.wordpress.com/2013/02/20/a-remarkable-discovery-all-solar-system-periods-fit-the-fibonacci-series-and-the-golden-ratio-why-phi/#:~:text=Since%20it%20was%20noticed%20that,structure%20of%20the%20solar%20system. - Accessed 22/06/22.
29. Pletser, V. Prevalence of Fibonacci numbers in orbital period ratios in solar planetary and satellite systems and in exoplanetary systems. *Astrophys. Space Sci.* **2019**, *364*. https://doi.org/10.1007/s10509-019-3649-2.
30. Broer, H.W. KAM theory: The legacy of Kolmogorov's 1954 paper. *Bull. Am. Math. Soc.* **2004**, *41*, 507–522. https://doi.org/10.1090/s0273-0979-04-01009-2.
31. Arnold, V.I. Proof of a theorem of A. N. Kolmogorov on the invariance of quasi-periodic motions under small perturbations of the Hamiltonian. *Russ. Math. Surv.* **1963**, *18*, 9–36. https://doi.org/10.1070/rm1963v018n05abeh004130.
32. Kibble, T.W.B.; Berkshire, F.H. *Classical Mechanics (5th Edition)*; Imperial College Press: London, 2004.
33. Dumas, H.S. *The KAM Story – A Friendly Introduction to the Content, History, and Significance of Classical Kolmogorov–Arnold–Moser Theory*; World Scientific: Singapore, 2014. https://doi.org/10.1142/8955.
34. Mitchison, G.J. Phyllotaxis and the Fibonacci Series. *Science* **1977**, *196*, 270–275. https://doi.org/10.1126/science.196.4287.270.
35. Douady, S.; Couder, Y. Phyllotaxis as a Dynamical Self Organizing Process Part I: The Spiral Modes Resulting from Time-Periodic Iterations. *J. Theor. Biol.* **1996**, *178*, 255–273. https://doi.org/10.1006/jtbi.1996.0024.
36. Naylor, M. Golden, $\sqrt{2}$, and π Flowers: A Spiral Story. *Math. Mag.* **2002**, *75*, 163–172. https://doi.org/10.1080/0025570x.2002.11953126.
37. Bergeron, F.; Reutenauer, C. Golden ratio and phyllotaxis, a clear mathematical link. *J. Math. Biol.* **2019**, *78*, 1–19. https://doi.org/10.1007/s00285-018-1265-3.
38. Güth, W.; Schmittberger, R.; Schwarze, B. An experimental analysis of ultimatum bargaining. *J. Econ. Behav. Organ.* **1982**, *3*, 367–388. https://doi.org/10.1016/0167-2681(82)90011-7.
39. Schuster, S. A New Solution Concept for the Ultimatum Game leading to the Golden Ratio. *Sci. Rep.* **2017**, *7*. https://doi.org/10.1038/s41598-017-05122-5.
40. Henein, M.Y.; Zhao, Y.; Nicoll, R.; Sun, L.; Khir, A.W.; Franklin, K.; Lindqvist, P. The human heart: Application of the golden ratio and angle. *Int. J. Cardiol.* **2011**, *150*, 239–242. https://doi.org/10.1016/j.ijcard.2011.05.094.
41. Tamargo, R.J.; Pindrik, J.A. Mammalian Skull Dimensions and the Golden Ratio (Φ). *J. Craniofac. Surg.* **2019**, *30*, 1750–1755. https://doi.org/10.1097/SCS.0000000000005610.
42. Shannon, G.; Marples, C.R.; Toofanny, R.D.; Williams, P.M. Evolutionary drivers of protein shape. *Sci. Rep.* **2019**, *9*. https://doi.org/10.1038/s41598-019-47337-8.

43. Penrose, R. Pentaplexity: A Class of Non-Periodic Tilings of the Plane. *Math. Intell.* **1979**, *2*, 32–37. https://doi.org/10.1007/bf03024384.
44. Grünbaum, B.; Shephard, G.C. *Tilings and Patterns*, second ed.; Dover Publications, Inc.: New York, 1986.
45. Ammann, R.; Grünbaum, B.; Shephard, G.C. Aperiodic tiles. *Discrete Comput. Geom.* **1992**, *8*, 1–25. https://doi.org/10.1007/bf02293033.
46. Shechtman, D.; Blech, I.; Gratias, D.; Cahn, J.W. Metallic Phase with Long-Range Orientational Order and No Translational Symmetry. *Phys. Rev. Lett.* **1984**, *53*, 1951–1953. https://doi.org/10.1103/physrevlett.53.1951.
47. Levine, D.; Steinhardt, P.J. Quasicrystals: A New Class of Ordered Structures. *Phys. Rev. Lett.* **1984**, *53*, 2477–2480. https://doi.org/10.1103/physrevlett.53.2477.
48. Levine, D.; Steinhardt, P.J. Quasicrystals. I. Definition and structure. *Phys. Rev. B* **1986**, *34*, 596–616. https://doi.org/10.1103/physrevb.34.596.
49. Socolar, J.E.S.; Steinhardt, P.J. Quasicrystals. II. Unit-cell configurations. *Phys. Rev. B* **1986**, *34*, 617–647. https://doi.org/10.1103/physrevb.34.617.
50. Bindi, L.; Steinhardt, P.J.; Yao, N.; Lu, P.J. Natural Quasicrystals. *Science* **2009**, *324*, 1306–1309. https://doi.org/10.1126/science.1170827.
51. Steinhardt, P.J.; Bindi, L. In search of natural quasicrystals. *Rep. Prog. Phys.* **2012**, *75*, 092601. https://doi.org/10.1088/0034-4885/75/9/092601.
52. Steinhardt, P.J. *The Second Kind of Impossible: The Extraordinary Quest for a New Form of Matter*; Simon & Schuster: New York, 2019.
53. Suresh, C.H.; Koga, N. A Consistent Approach toward Atomic Radii. *J. Phys. Chem. A* **2001**, *105*, 5940–5944. https://doi.org/10.1021/jp010432b.
54. Heyrovska, R. The Golden ratio, ionic and atomic radii and bond lengths. *Mol. Phys.* **2005**, *103*, 877–882. https://doi.org/10.1080/00268970412331333591.
55. Heyrovska, R. Golden ratio based fine structure constant and Rydberg constant for hydrogen spectra. *Int. J. Sci.* **2013**. Available at SSRN: https://ssrn.com/abstract=2572314.
56. Prialnik, D. *An Introduction to the Theory of Stellar Structure and Evolution, 2nd Edition*; Cambridge University Press: Cambridge, 2009.
57. Davies, P.C.W. The thermodynamic theory of black holes. *Proc. R. Soc. A* **1977**, *353*, 499–521. https://doi.org/10.1098/rspa.1977.0047.
58. Davies, P.C.W. Thermodynamic phase transitions of Kerr-Newman black holes in de Sitter space. *Class. Quantum Gravity* **1989**, *6*, 1909–1914. https://doi.org/10.1088/0264-9381/6/12/018.
59. Baez, J.C. Black Holes and the Golden Ratio, 2013. Available at: https://johncarlosbaez.wordpress.com/2013/02/28/black-holes-and-the-golden-ratio/ - Accessed 26/02/20.
60. Cruz, N.; Olivares, M.; Villanueva, J.R. The golden ratio in Schwarzschild–Kottler black holes. *Eur. Phys. J. C* **2017**, *77*. https://doi.org/10.1140/epjc/s10052-017-4670-7.
61. Gross, D.J.; Harvey, J.A.; Martinec, E.; Rohm, R. Heterotic String. *Phys. Rev. Lett.* **1985**, *54*, 502–505. https://doi.org/10.1103/physrevlett.54.502.
62. Lisi, A.G. An Exceptionally Simple Theory of Everything, 2007. https://doi.org/10.48550/ARXIV.0711.0770.
63. Lisi, A.G.; Weatherall, J.O. A Geometric Theory of Everything. *Sci. Amer.* **2010**, *303*, 54–61.
64. Garibaldi, S. E_8, the most exceptional group. *Bull. Am. Math. Soc.* **2016**, *53*, 643–671. https://doi.org/10.1090/bull/1540.
65. Viazovska, M. The sphere packing problem in dimension 8. *Ann. Math.* **2017**, *185*. https://doi.org/10.4007/annals.2017.185.3.7.
66. Coldea, R.; Tennant, D.A.; Wheeler, E.M.; Wawrzynska, E.; Prabhakaran, D.; Telling, M.; Habicht, K.; Smeibidl, P.; Kiefer, K. Quantum Criticality in an Ising Chain: Experimental Evidence for Emergent E_8 Symmetry. *Science* **2010**, *327*, 177–180. https://doi.org/10.1126/science.1180085.
67. Zamolodchikov, A.B. Integrals of motion and S-matrix of the (scaled) T = T_c Ising model with magnetic field. *Int. J. Mod. Phys. A* **1989**, *04*, 4235–4248. https://doi.org/10.1142/s0217751x8900176x.
68. Affleck, I. Golden ratio seen in a magnet. *Nature* **2010**, *464*, 362–363. https://doi.org/10.1038/464362a.
69. Boeyens, J.C.; Thackeray, J.F. Number theory and the unity of science. *S. Afr. J. Sci.* **2014**, *110*, 1–2. https://doi.org/10.1590/sajs.2014/a0084.
70. Irwin, K.; Amaral, M.M.; Aschleim, R.; Fang, F. Quantum walk on spin network and the golden ratio as the fundamental constant of nature. In Proceedings of the Fourth International Conference on the Nature and Ontology of Spacetime, C16-05-30.9, 2017, pp. 117–160.